6-1971

Design and application of a photon-coupled isolator circuit for Langmuir probe instrumentation.

Roy L. Heifner
University of Tennessee

To the Graduate Council:

I am submitting herewith a thesis written by Roy L. Heifner entitled "Design and application of a photon-coupled isolator circuit for Langmuir probe instrumentation.." I have examined the final electronic copy of this thesis for form and content and recommend that it be accepted in partial fulfillment of the requirements for the degree of Master of Science, with a major in Electrical Engineering.

Fred M. Shofner, Major Professor

We have read this thesis and recommend its acceptance:

Accepted for the Council:
Carolyn R. Hodges

Vice Provost and Dean of the Graduate School

(Original signatures are on file with official student records.)

March 1, 1971

To the Graduate Council:

I am submitting herewith a thesis written by Roy L. Heifner, Jr. entitled "Design and Application of a Photon-Coupled Isolator Circuit for Langmuir Probe Instrumentation." I recommend that it be accepted for nine quarter hours of credit in partial fulfillment of the requirements for the degree of Master of Science, with a major in Electrical Engineering.

Fred M. Strohmer
Major Professor

We have read this thesis
and recommend its acceptance:

K Ehn

E C Auerbachmann

Accepted for the Council:

Hilton A. Smith
Vice Chancellor for
Graduate Studies and Research

DESIGN AND APPLICATION OF A PHOTON-COUPLED ISOLATOR CIRCUIT FOR LANGMUIR PROBE INSTRUMENTATION

A Thesis

Presented to

the Graduate Council of

The University of Tennessee

In Partial Fulfillment

of the Requirements for the Degree

Master of Science

---

by

Roy L. Heifner, Jr.

June 1971

ACKNOWLEDGMENT

The author wishes to express his appreciation to his major professor, Dr. F. M. Shofner, for the opportunity to work on this project and for his direction and assistance throughout its course. Special thanks are due two fellow students, D. W. Turner for his suggestions in the early phases of this study and T. B. Carlson, whose advice and assistance during the application phase proved invaluable. To all his professors and fellow students, the author expresses his thanks for a fruitful and enjoyable association.

The author also expresses his gratitude to his wife, Pat, and daughter, Lisa. Their encouragement and patient endurance is greatly appreciated.

The research described in this thesis was supported financially by National Science Foundation grant GK-2252.

ABSTRACT

The analysis and design of a photon-coupled isolator circuit and its application for obtaining swept Langmuir probe characteristics of a plasma are presented. Swept probe characteristics for a low pressure plasma are given and electron temperature and density are determined. The circuit is also used to measure plasma fluctuations in a double probe experiment.

TABLE OF CONTENTS

LIST OF FIGURES

FIGURE PAGE

NOMENCLATURE

A_s	Probe area
A_{vt}	Voltage gain
b'	Internal base terminal
$C_{b'c}$	Capacitance from b' to collector
$C_{b'e}$	Capacitance from b' to emitter
C_{DG}	Capacitance from drain to gate
C_{SG}	Capacitance from source to gate
e	Electronic charge
G	Photon-coupled isolator current transfer ratio
GaAs	Galium arsenide diode
g_m	Bipolar transistor transconductance
g_{fs}	FET transconductance
h_{ie}	Small signal hybrid parameter
I_{DSS}	Gate-to-source short circuit drain current
I_P	Total probe current
k	Boltzmann's constant
LED	Light emitting diode
ℓn	Natural logarithm
m_e	Electronic mass
n_{ep}	Plasma electron density
PCI	Photon-coupled isolator
T_e	Electron temperature, degrees Kelvin
V_f	Floating potential
V_P	FET pinchoff voltage, probe voltage

V_S	Plasma space potential
β	Small signal CE short-circuit current gain

CHAPTER I

INTRODUCTION

The study of plasmas has been greatly accelerated in recent years (1)[1] due to the interest in such topics as controlled thermonuclear reactors, magnetohydrodynamic generators, gas lasers and plasma propulsion systems for space travel. Among the most important experimental parameters, if not the most important which are measurable, are electron density and temperature (2-5). A fundamental technique and the first to be used for measuring these properties is that of an electrostatic probe developed by Langmuir in 1924. Although other diagnostic methods, such as the use of microwaves or spectroscopy, have been developed, their use is generally limited and serves to supplement the Langmuir probe. In addition to simplicity the Langmuir probe is advantageous over other diagnostic techniques in that time and space resolved measurements can be made (5). The techniques developed by Langmuir are still the basis for examining low pressure discharges (1).

In the introduction to his book, Huddlestone (5) proposes an excellent statement of the problem and objective for plasma instrumentation: "An important ingredient in

---

[1]Numbers in parentheses refer to similarly numbered references in the bibliography.

generating a plasma and studying this poorly behaved state of matter is a highly developed instrumentation for monitoring and measuring the very difficult and usually transient conditions under which most laboratory plasmas exist. Many diagnostic techniques require good time resolution in the microsecond and even nanosecond range, careful discrimination to achieve acceptable signal-to-noise levels and stringent material requirements to achieve acceptable levels of plasma purity." To develop such instrumentation which exploits the good transient response of the Langmuir probe in the retarding field region and which provides the probe characteristic isolated from the high dc voltage of the plasma was the purpose of this research.

A major source of errors with Langmuir probe measurements is the nonrepeatability attributed to changing surface conditions of the probe due to contamination (6, 7). The probe characteristic has been found to be very repeatable, however, if the measurement is made on the order of one second after the probe has been discharge cleaned (7). The transient response of the retarding probe itself was found to be of the order 10^{-8} seconds (8) or a frequency response of 35 MHz. Shofner, Bray and Carlson (9) found the spectrum of intrinsic plasma noise to decay rapidly after a break point at less than 100 kHz. Therefore, if the probe is clean, reliable measurements of transient plasma properties should be possible if the probe and associated instrumentation circuitry have a frequency response of more than

100 kHz.

The procedure for obtaining the Langmuir probe characteristic is to measure the voltage drop across a resistance in series with the probe as the probe voltage is varied with respect to the plasma potential. The instrumentation must distinguish millivolt variations of the probe characteristic about average potentials which may be several thousand volts. It must also provide the necessary isolation so that probe characteristics may be safely and conveniently recorded by an oscilloscope or other recording device.

Shofner (10) studied a voltage-controlled tunnel diode oscillator circuit (frequency modulation) which provided isolation by electromagnetic coupling of 10.7 MHz radiation. This circuit had good frequency response and sensitivity, but was limited due to bias stability problems of the oscillator. He later (1966) designed a simple photon-coupled isolator circuit which has been successfully applied in the acquisition of magnetohydrodynamic generator current fluctuations and has voltage isolation between the input and output of 10,000 volts. This circuit has been further investigated by Welch (11). The input of the isolator consists of a gallium arsenide light emitting diode (LED) which emits infrared light in proportion to its forward current. The radiation is guided by a light pipe to a silicon PIN photodiode. The current in the photodiode is proportional to the intensity of the light incident upon it.

The output is therefore controlled by, but isolated from, the input. Photon-coupled isolators are available which have breakdown voltages up to 50 KV and current transfer cutoff frequencies of 10 MHz (12). Utilization of the photon-coupled isolator for Langmuir probe instrumentation thus provides both the high voltage isolation and the transient response for conveniently recording the probe characteristic.

Chapter II is a discussion of the design and analysis of the circuitry for use with the photon-coupled isolator. The mid-frequency gain and the high-frequency break point for the circuit are both calculated and measured.

Chapter III provides an experimental verification and application of the photon-coupled isolator circuit in Langmuir probe diagnostics. Basic probe theory is presented. Oscilloscope traces of probe characteristics for low pressure helium discharges were photographed and are included. Also included are double probe plasma noise measurements made for varying pressures, discharge currents, and distances between probes.

Chapter IV gives the conclusions drawn from the research and suggested improvements for the photon-coupled isolator circuit.

CHAPTER II

CIRCUIT ANALYSIS

I. CIRCUIT DESCRIPTION

The schematic diagram of the complete photon-coupled isolator circuit is shown in Figure 1. The photon-coupled isolator selected for this application is the Hewlett Packard Associates hpa 4303. Selection was based on isolation and frequency response characteristics. The hpa 4303 has a current transfer ratio of approximately 3×10^{-4} and a current transfer cut-off frequency of 7 MHz. It can withstand up to 20,000 volts between the input and output (12). The transfer characteristics are rated at 25 °C and are extremely temperature dependent.

Input and output circuits are required for use with the photon-coupled isolator. The input, or driver, circuit senses the Langmuir probe signal and produces an output current proportional to the millivolt variations developed across the source impedance. The output circuit is essentially a pre-amplifier which converts the high impedance signal from the photodiode to a signal usable by one of the recording devices.

Drive Circuit

A Field-Effect Transistor (FET) was selected for the driver circuit because it provides a gain essentially

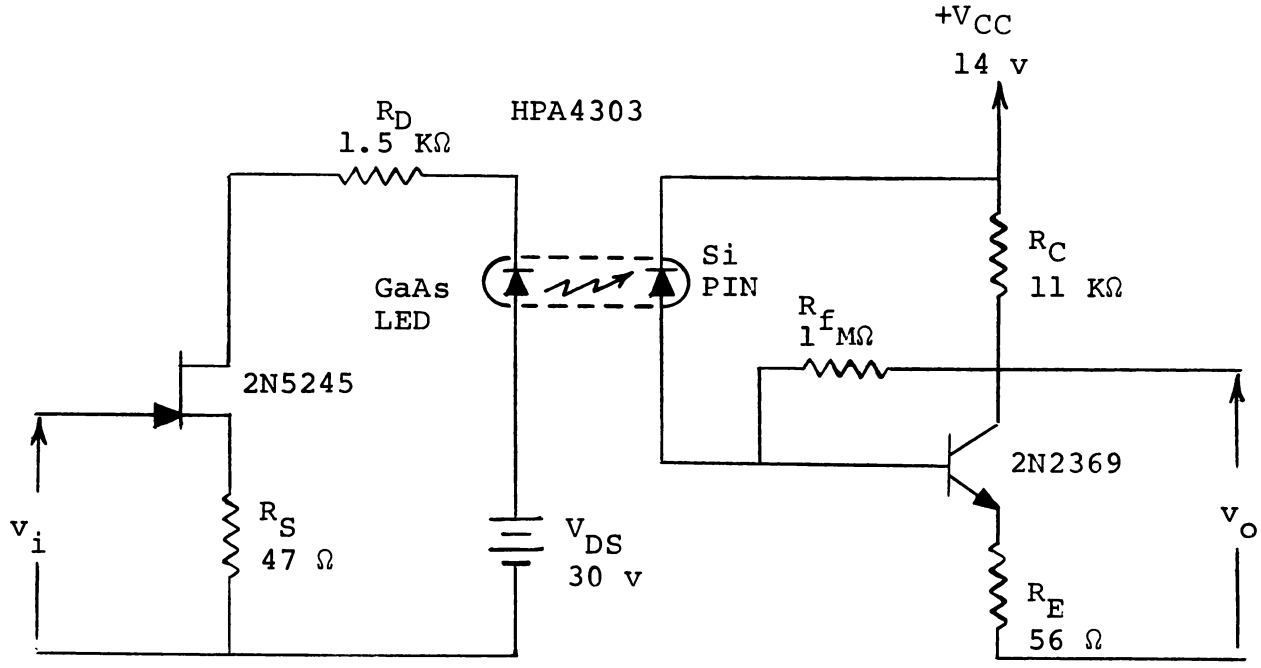

Figure 1. Schematic of the photon-coupled isolator circuit.

independent of the input impedance, since negligible gate current is drawn. A Texas Instruments 2N5245 N-Channel silicon FET was selected because it provides the desirable gain and frequency response, and proper current to drive the LED (13). That the characteristics of the 2N5245 FET vary widely from device to device was apparent from the data sheets and was shown to be the case in the laboratory. Approximately one-third of the devices tested exhibited drain current characteristics satisfactory for use with the photon-coupled isolator. Drain characteristics were determined using a Tektronic Curve Tracer and are shown in Figure 2.

The forward transfer curve for the 2N5245 can be determined from the drain characteristics. The forward transfer curve is nonlinear and is quite accurately approximated by the quadratic relationship (14-16)

$$I_D = I_{DSS}\left(1 - \frac{V_{GS}}{V_P}\right)^2 \qquad (1)$$

where I_{DSS} is the drain current for a gate-to-source short circuit, V_{GS} is the dc source-to-gate voltage, and V_P is the drain current pinch-off voltage. From this curve and the current requirements of the LED, a quiescent operating point was chosen along with the corresponding drain power supply voltage, V_{DD}, and the required source-to-gate bias voltage, V_{GS}, was determined.

The drain characteristic curves for increments of V_{GS}

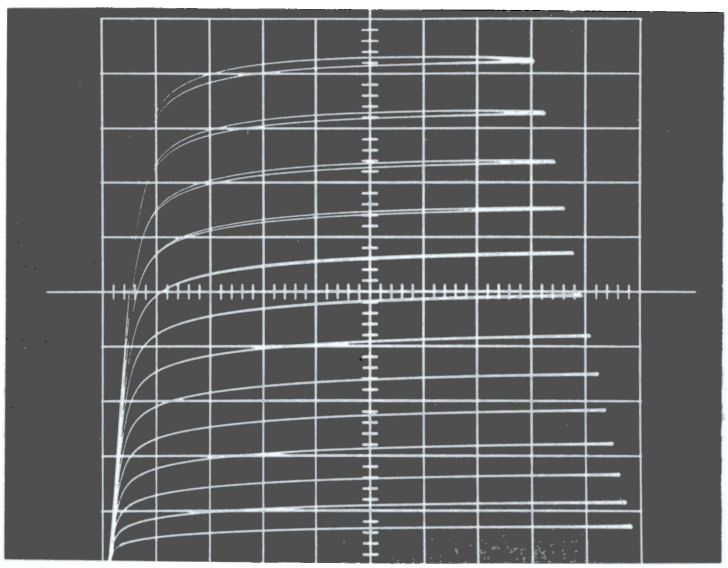

Vertical: 1 ma/cm

Horizontal: 5 v/cm

Gate Steps: 0.2 v

Figure 2. Common source characteristics for the 2N5245 FET.

near pinch-off change very slowly and make the value of V_P difficult to read directly from the curves. However, V_P can be inferred by measuring V_{GS} at some drain current less than I_{DSS} and calculating the value from Equation 1. A convenient relationship which is used frequently (14, 16) is

$$V_P = 1.46\ V_{GS}\Big|_{I_D = 0.1\ I_{DSS}} \tag{2}$$

For the 2N5245 used here, I_{DSS} was found to be 9 milliamps. The quiescent operating point along with the proper source-to-gate bias resistor, R_S, were determined experimentally. However, the equations can provide design guidance and indicate limits for the input signal. Using the value of I_{DSS} = 9 milliamps and V_{GS} = -2.1 volts for $I_D = 0.1\ I_{DSS}$, Equation 2 yields

$$V_P = (1.46)(-2.1) = -3.1 \text{ volts} \tag{3}$$

In order that the photon-coupled isolator operate in its linear region a minimum I_D of 5 milliamps is required (11). Using this value and the anticipated value of the input voltage a V_{GS} = 0.35 volts was selected using the transfer curve. This value of V_{GS} will insure operation in the linear portion of the photon-coupled isolator's forward transfer characteristic as well as in the linear portion of the FET forward transfer curve. It was found experimentally that the maximum positive source-to-gate voltage which could be applied was approximately one volt. Exceeding this value

results in a power dissipation which is too great (12) and the FET is damaged. However, the maximum anticipated input for the Langmuir probe studies was a few hundred millivolts and, therefore, this limitation of V_{GS} was no problem.

The negative bias required for the gate of the FET is achieved with the resistor R_S. Using the values determined experimentally for I_{DSS} and V_P, and the selected value of V_{GS}, the quiescent drain current is found from Equation 1 as

$$I_D = (9)(10^{-3})\left(1 - \frac{(-0.35)}{(-3.1)}\right)^2 = 7.0 \text{ milliamps} \qquad (4)$$

Under quiescent conditions, with the input signal equal zero, $V_{GS} = R_S I_D$ and R_S needed to bias the FET at the selected quiescent point is

$$R_S = \frac{V_{GS}}{I_D} = \frac{0.35 \text{ volts}}{7.0 \text{ milliamps}} = 50 \text{ ohms} \qquad (5)$$

The maximum steady current for the LED recommended by the manufacturer is 70 milliamps at 25 °C (12). It has been shown (11) that currents in excess of 50 milliamps can result in damage to the LED. The resistor, R_D = 1.5 kilohm was added to limit the drain current to a safe level.

Preamplifier Circuit

The 2N2369 NPN silicon transistor has been used in a similar circuit (11, 17) and was selected for the pre-amplifier circuit because of its high speed and temperature

stability. Biasing arrangements had been determined for a similar circuit (11) used with the photon-coupled isolator and were duplicated here as a starting point. The resistors R_f and R_C were determined experimentally to give optimum gain. A potentiometer was placed in series with each and the desired resistance value was determined.

Common emitter characteristics for the 2N2369 transistor obtained using the Tektronic curve tracer are shown in Figure 3. The value of the forward current transfer ratio, β, was determined from the curves to be 60.

II. CALCULATED CIRCUIT GAIN

The basic FET amplifier in common-source configuration with source resistor is shown in Figure 4 with its equivalent circuit. The FET's forward transconductance, which is the slope of the transfer characteristic curve for the given bias condition is defined by (14-16)

$$g_{fs} = \frac{dI_D}{dV_{GS}} \tag{6}$$

Using the quadratic approximation of Equation 1 for I_D and differentiating with respect to V_{GS} gives (15, 16)

$$g_{fs} = \frac{2I_{DSS}}{V_P}\left(1 - \frac{V_{GS}}{V_P}\right) \tag{7}$$

Substituting values into Equation 7 gives

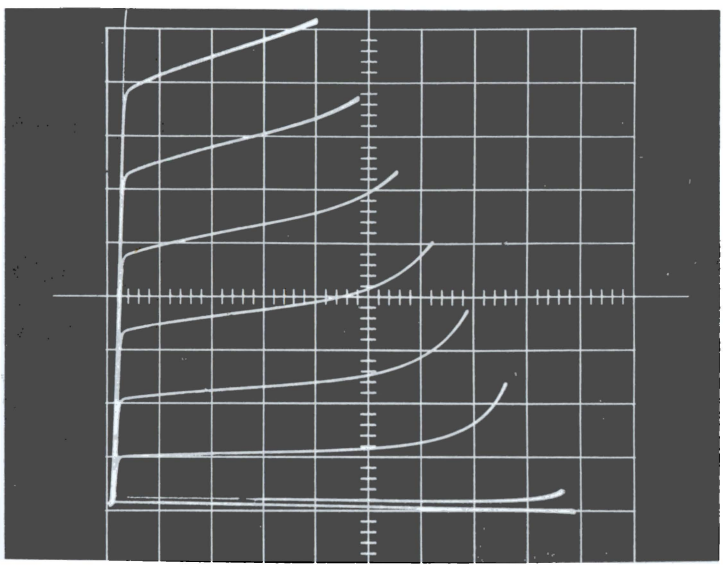

Vertical: 0.2 ma/cm

Horizontal: 2 v/cm

Base Steps: 5 μa

Figure 3. Common emitter characteristics for the 2N2369 transistor.

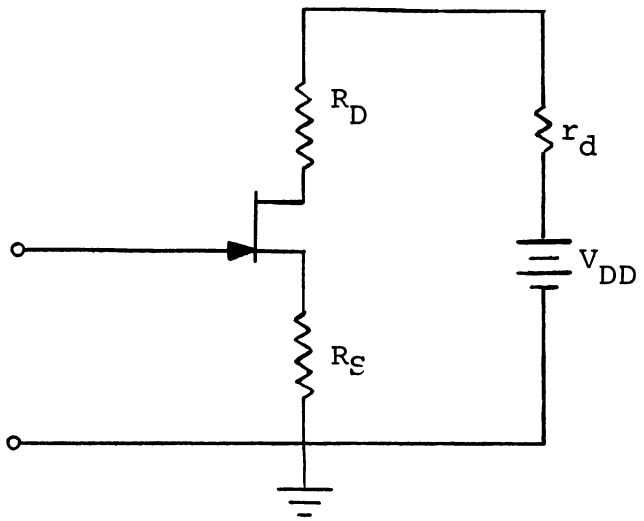

(a) Circuit diagram

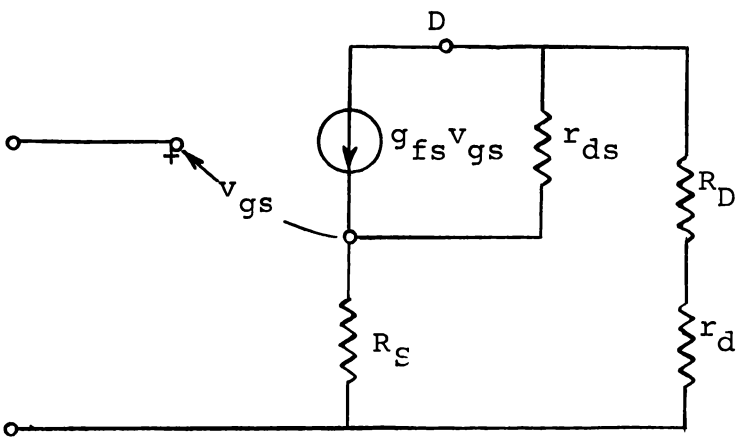

(b) Simplified equivalent circuit

Figure 4. Common source FET amplifier with a source resistor.

$$g_{fs} = \frac{(-2)(9)(10^{-3}) \text{ amps}}{(3.1) \text{ volts}}\left(1 - \frac{(-0.35)}{(-3.1)}\right)$$

$$= 5.1 \text{ millimhos} \tag{8}$$

Since the LED emits light proportional to its forward current the gate-voltage-to-drain-current transfer function should give the gain in the driver circuit. Since the source resistor R_S actually introduces negative feedback, the value for g_{fs} found by Equation 8 must be modified. The total drain current is given by

$$I_d = I_D + g_{fs} v_{gs} \tag{9}$$

where I_D is the DC component of drain current, v_{gs} is the instantaneous source-to-gate AC voltage, and $g_{fs}v_{gs}$ is the AC component of drain current, i_d. Assuming that the gate current is negligible and that we can neglect any drop across the signal source, v_{gs} is given by

$$v_{gs} = v_i + i_d R_S \tag{10}$$

Substituting Equation 10 into Equation 9 and dropping the DC component yields

$$i_d = g_{fs}(v_i + i_d R_S) \tag{11}$$

Solving for i_d/v_i gives an effective transconductance for the amplifier with source resistor (16)

$$\frac{i_d}{v_i} = g'_{fs} = \frac{g_{fs}}{1 + g_{fs}R_S}$$

$$= \frac{(5.1)(10^{-3})}{1 + (5.1)(10^{-3})(47)} = 4.1 \text{ millimhos} \qquad (12)$$

Figure 5 shows a simplified circuit for the mid-frequency gain calculation. The photodiode is represented by an equivalent current generator where G is the current transfer ratio of the photon-coupled isolator and i_d is the current in the LED (and the FET). The circuit is analyzed by treating the base as a summing point for the input current and that part of the output current which flows through the feedback resistor, R_f (18). The base current is the difference between i_i and i_f. The voltage drop across R_f is

$$v_f = v_i - v_o \qquad (13)$$

The output is taken across the resistor, R_C, and is given by

$$v_o = -(i_c - i_f)R_C \qquad (14)$$

But since $R_f >> R_C$, $i_f << i_c$, and the output voltage may be approximated by

$$v_o \simeq -i_c R_C = -\beta i_b R_C \qquad (15)$$

which is the same voltage as in the absence of the feedback resistor. An effective input resistor can be defined as

$$R_{fi} = \frac{v_i}{i_f} = \frac{v_i}{(v_i - v_o)/R_f} = \frac{R_f}{\left(1 - \frac{v_o}{v_i}\right)} = \frac{R_f}{1 - A_{vt}} \qquad (16)$$

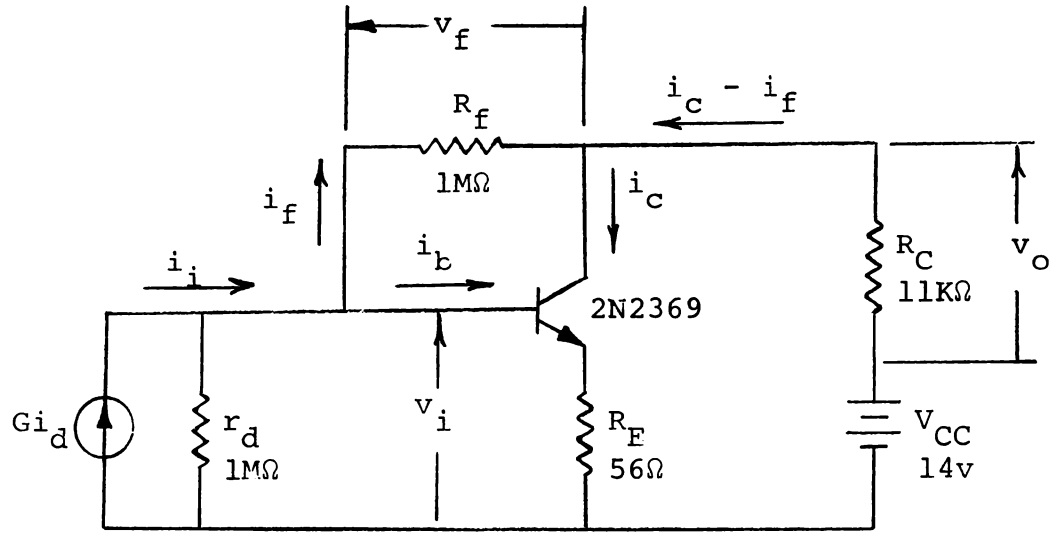

Figure 5. Simplified circuit for calculation of mid-band gain.

where A_{vt} is the terminal voltage gain calculated according to the equivalent circuit shown in Figure 6.

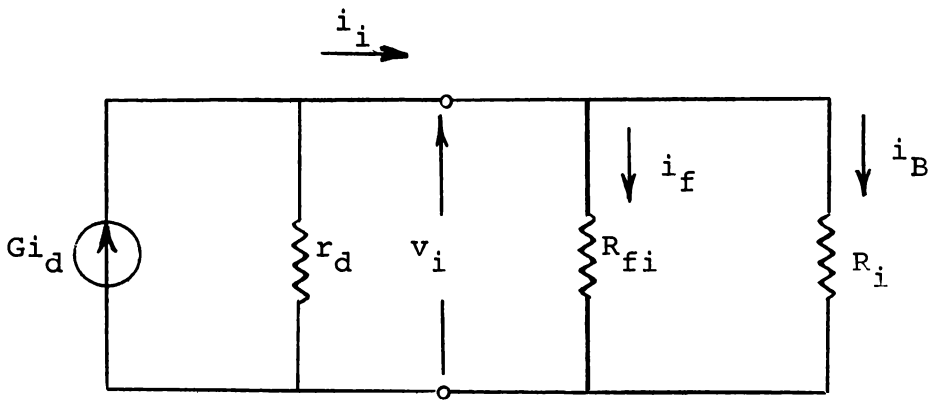

Figure 6. Mid-band AC equivalent circuit.

Note that the feedback resistor R_E must be included in the gain calculation:

$$A_{vt} = \frac{v_o}{v_i} \simeq - \frac{\beta i_b R_C}{i_b R_i} \tag{17}$$

where R_i is the effective input resistance.

$$R_i = h_{ie} + (\beta + 1)R_E = 2 \times 10^3 + (60 + 1)56$$

$$= 5.4 \times 10^3 \tag{18}$$

Thus

$$A_{vt} = \frac{-60 \times 11}{5.4} = -122$$

and

$$R_{fi} = \frac{10^6}{123} = 8.2\ K\Omega$$

A relation for the base current i_b in terms of the current in the PIN photodiode may now be found. Using current division and neglecting r_d as large

$$i_b = G_{id} \frac{R_{fi}}{R_{fi} + R_i} = 0.6\ G_{id} \tag{19}$$

The expression for the output voltage is thus given by

$$v_o = -\beta R_C \frac{R_{fi}}{R_{fi} + R_i} G\ g'_{fs}\ v_i \tag{20}$$

The manufacturer's data sheets for the photon-coupled isolator (12) advertise a transfer function, G, of 3×10^{-4}, rated at a current of 25 milliamps through the GaAs LED. This transfer function was measured and found to vary with LED current. Figure 7 shows the measured transfer function at lower currents. For an LED current of 7 milliamps, which is the driver circuit quiescent current, G was measured to be 2.5×10^{-3}. Substituting this value of G and the numerical values determined above into Equation 20 yields

$$v_o = +0.40\ v_i \tag{21}$$

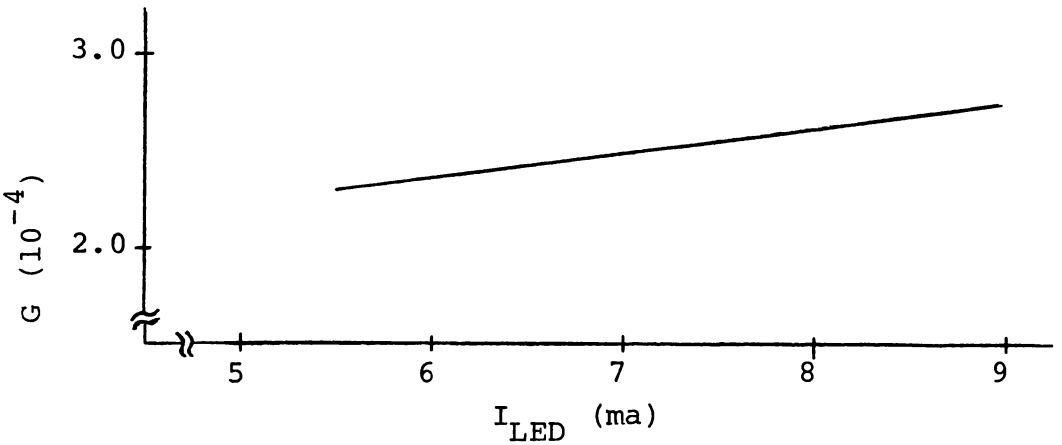

Figure 7. Transfer function of the photon-coupled isolator as a function of LED current.

III. CALCULATED CIRCUIT FREQUENCY RESPONSE

The frequency response analysis of the circuit is made in two parts. The high-frequency break point is determined first for the driver circuit and then for the preamplifier circuit. The frequency response of the photon-coupled isolator is limited by the photon emission time constant of the GaAs LED (17). The manufacturer's specification sheet (12) gives a high-frequency break point (-3db) of 7 MHz.

A high-frequency equivalent circuit for the driver is shown in Figure 8 (14). The unbypassed source resistor is small and since its presence extends the high-frequency response (18) it can be eliminated for a worse-case analysis. The high-frequency break point for this input is found from

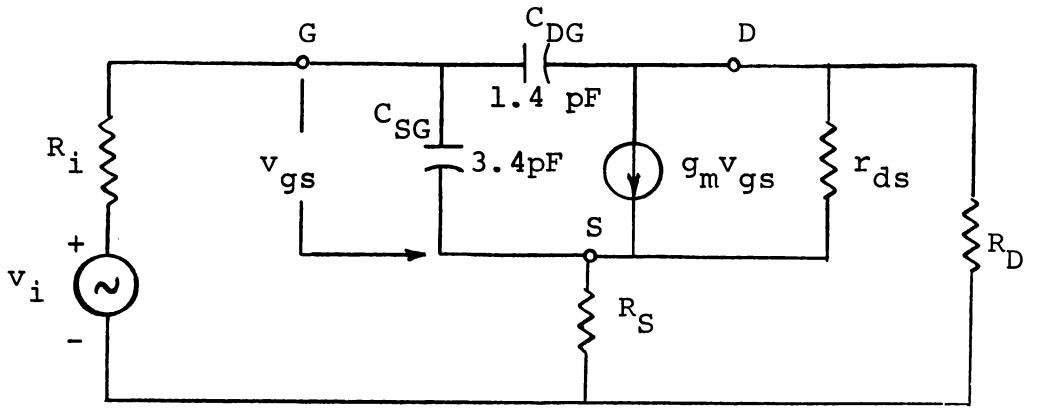

Figure 8. High-frequency equivalent for the driver circuit.

$$f_{i_1} = \frac{1}{2\pi RC} \tag{22}$$

where R is the parallel combination of R_D and r_{ds}, and C is the input capacitance

$$C = C_{SG} + C_{DG}(1 - A_{vt}) \tag{23}$$

The drain-to-gate capacitance appears multiplied because the FET in common source configuration is subject to the Miller effect just as the transistor is in common-emitter circuits (14). Since r_{ds} is on the order of 100 Kilohms, $R \simeq R_D$ = 1.5 Kilohms. From Equation 23,

$$C = 3.4 + 1.4(1 + 6.1) = 13.3 \text{ picofarads} \tag{24}$$

where A_{vt} was found from

$$A = -g'_{fs}R_D = -4.1 \times 1.5 = -6.1 \tag{25}$$

The high-frequency break point is

$$f_{i_1} = \frac{1}{2\pi(1.5)(10^3)(13.3)(10^{-12})} = 8 \text{ MHz} \tag{26}$$

For the output break point R is R_D and C is C_{DG} and

$$f_{o_1} = \frac{1}{2\pi(1.5)(10^3)(1.4)(10^{-12})} = 76 \text{ MHz} \tag{27}$$

The function of R_D was to provide protection. Since the resistance of the forward biased diode is very low, $\approx$ 1Ω, the frequency response of the driver stage could be extended significantly. However, it will be seen that the output amplifier is limiting and there was no point in reducing R_D.

Figure 9 is the high-frequency equivalent for the pre-amplifier circuit. Neglecting r_b, the break point for the input is determined by the parallel combination of r_d, R_{f_i} and R_i which is 3.2 KΩ and the capacitance which shunts it,

$$C = C'_{b'e} + C_{b'c}(1 - A_{vt})$$

$$= C_{b'e}\frac{r_e}{R_f + r_e} + C_{b'c}(1 + g_m R_{eq})$$

$$= 2.5 \text{ pF} + 3 \text{ pF}(123) = 372 \text{ pF} \tag{28}$$

The input high-frequency break point is

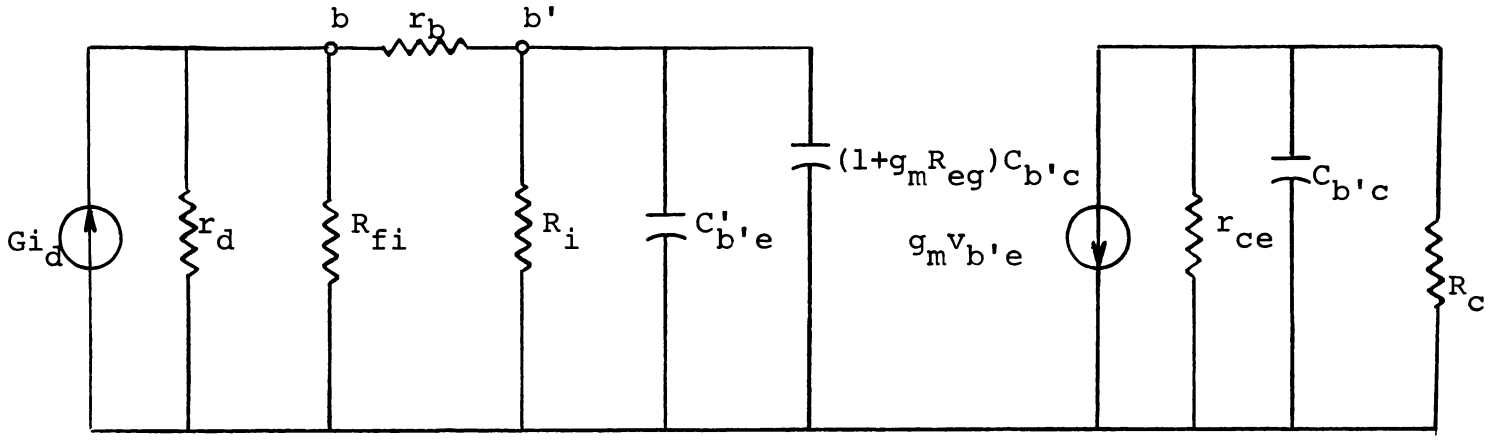

Figure 9. High-frequency equivalent for the preamplifier circuit.

$$f_{i2} = \frac{1}{2\pi(3.2 \times 10^{3})(372)(10^{-12})} \simeq 130 \text{ kHz} \qquad (29)$$

For the output break point

$$R \simeq R_C = 11 \text{ Kilohms}$$

$$C \simeq C_{b'c} + C_{scope} + C_{stray} = 3pF + 15pF + 10pF = 28pF$$

and

$$f_{o_2} = \frac{1}{2\pi(11 \times 10^{3})(28 \times 10^{-12})} \simeq 500 \text{ kHz} \qquad (30)$$

IV. MEASURED CIRCUIT PERFORMANCE

Theoretical and measured gain and frequency response for the photon-coupled isolator circuit are shown in Figure 10.

Equation 28 shows the effect of the load resistor on the high-frequency break point for the preamplifier circuit. In the preliminary design of this circuit a load resistor of 1.5 kilohms was used. The gain of the circuit was approximately 0.1 with a frequency response to about 1 MHz. As will be shown in Chapter III, plasma noise detected by the Langmuir probe was found to have frequencies below 100 Kilohertz. The load resistor was changed to get higher gain with a frequency response of approximately 100 kHz.

The effects of temperature changes on the circuit were also measured. Figure 11 is a plot of gain versus

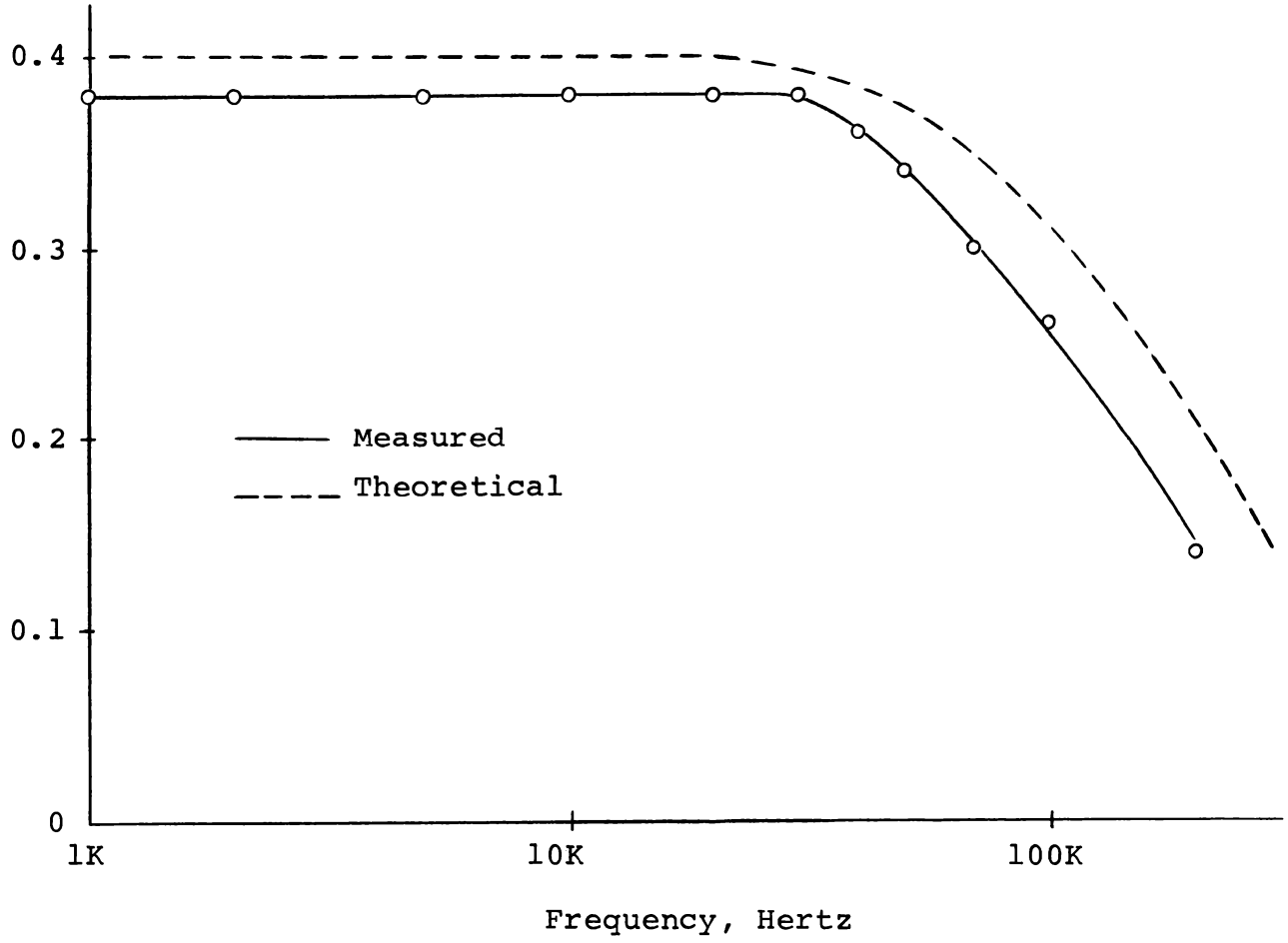

Figure 10. Theoretical and measured gain and frequency response.

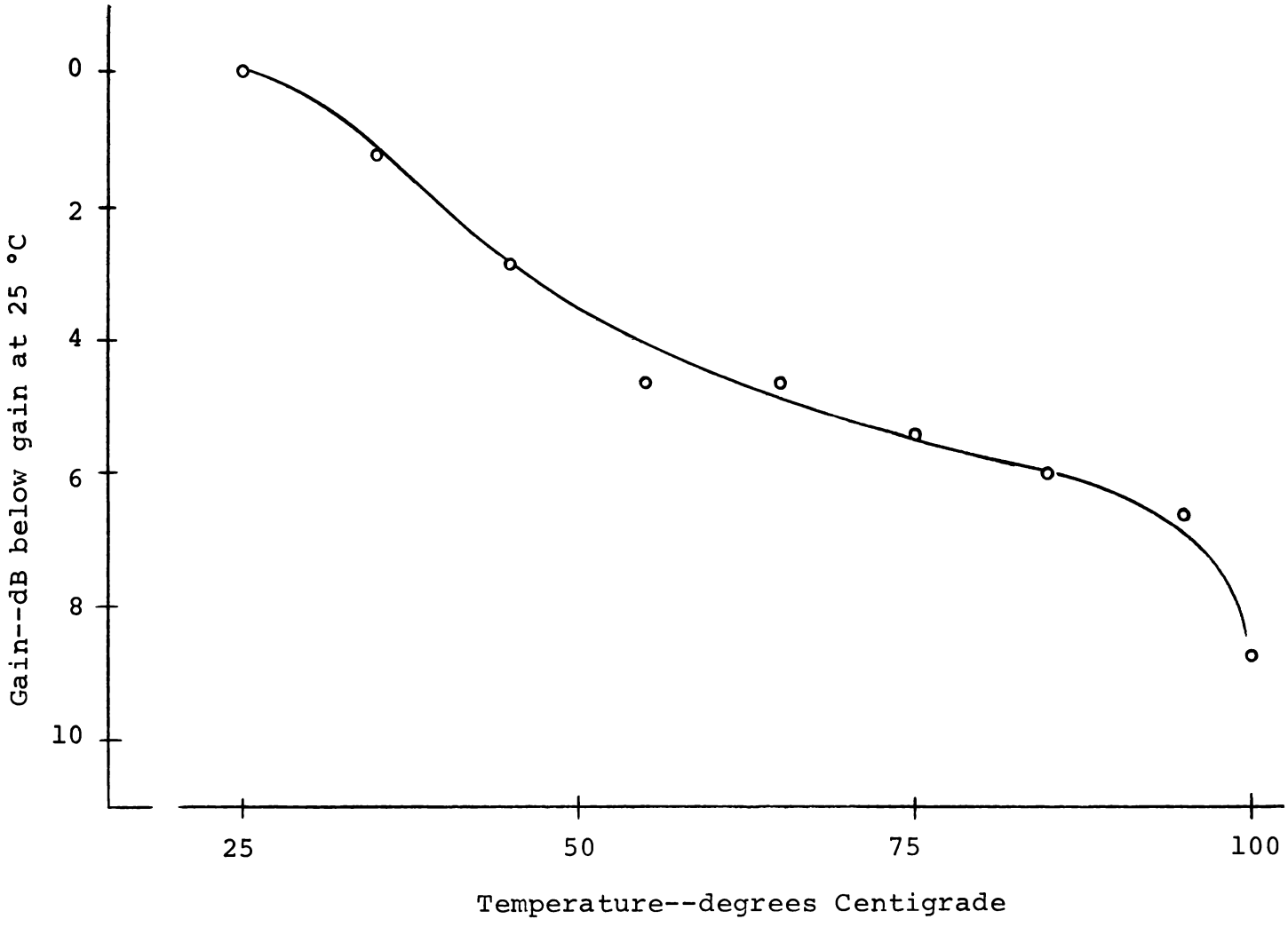

Figure 11. Variation of gain with temperature for the photon coupled isolator.

temperature which shows the strong temperature dependence of the circuit. This problem is currently under investigation by D. W. Turner as another thesis research project.

CHAPTER III

APPLICATION OF THE PHOTON-COUPLED ISOLATOR TO LANGMUIR PROBE PLASMA DIAGNOSTICS

I. BASIC PROBE THEORY

The principles and theory of Langmuir probes are well covered in the literature from the early works of Langmuir and others (19-21) to the recent texts by Huddlestone and Leonard (5), and Cobine (1). The purpose here is to show only the basic theory of probe volt-ampere characteristics and how useful plasma parameters can be determined from them.

Basically, the Langmuir probe is a small metallic electrode inserted into the plasma. The probe is connected to a power supply which is capable of biasing it in a range of voltages both positive and negative with respect to the potential of the surrounding plasma. Figure 12 shows the circuit for obtaining the Langmuir probe characteristic and a plot of a typical probe characteristic. The probe voltage is plotted with respect to the voltage V_S, called the space potential. At $V_P = V_S$ the particles striking the probe do so because of their thermal velocities. Electrons, because of their small mass, have much greater velocities than the ions and therefore the probe current is predominantly electron current. If the probe voltage is increased from

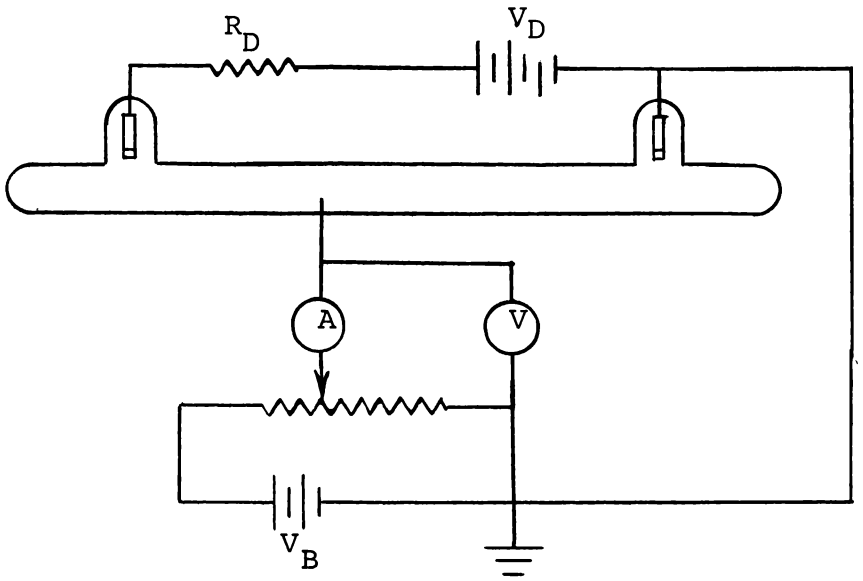

(a) Circuit for obtaining Langmuir probe characteristic

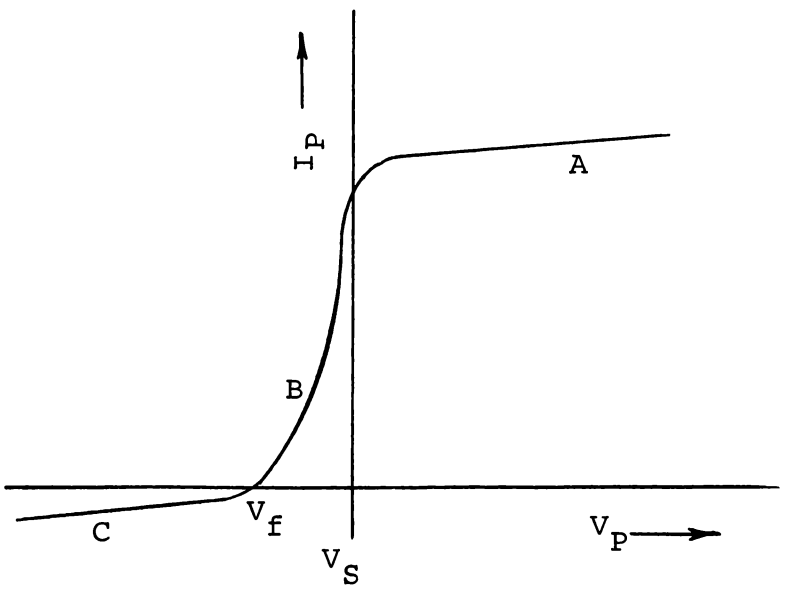

(b) Typical Langmuir probe characteristic

Figure 12. Langmuir probe characteristics.

V_S, electrons are attracted toward the probe and ions are repelled. The small amount of ion current which was present at V_S disappears. Because of an excess of electrons, an electron space-charge sheath is built up around the probe. Fortunately, the sheath is usually very thin and very little electric field exists outside the sheath, so that the plasma is undisturbed. The probe current in this region consists of electrons which penetrate the sheath by their random thermal velocities. This region (region A in Figure 12b) is fairly flat and is called the saturation electron region.

In the region B, as the probe is made more negative than V_S, electrons begin to be repelled and ions are attracted. A positive ion space charge sheath is built up around the probe. If the velocity distribution for the electrons is Maxwellian, the curve in this region, called the retarding field region, is exponential after the small ion current is subtracted. At the point V_F, called the floating potential, the probe has been made sufficiently negative to repel all the electrons except a number equal to the number of ions which are collected and, therefore, the net probe current is zero. If the probe is made more negative (region C) almost all the electrons are repelled and a saturation ion current exists.

The shape of the characteristic curve in the retarding field region is related to the electron energy distribution. If the electron velocities have a Maxwellian distribution, the Boltzmann relation may be used to determine the electron

density n_{es} at the probe surface in terms of the electron density n_{ep} at the plasma boundary of the sheath. The equation is 31

$$n_{es} = n_{ep} \exp\left(\frac{eV}{kT_e}\right) \tag{31}$$

where T_e is the absolute temperature of the plasma electrons and $V = V_P - V_S$, the potential of the probe relative to that of the plasma. The random plasma electron current density is

$$j_{ep} = \frac{1}{4} n_{ep} e v_{ep} \tag{32}$$

and the electron current density j_{es} to the probe is given by a similar expression. The electron current density to the probe is

$$j_{es} = j_{ep} \exp\left(\frac{eV}{kT_e}\right) \tag{33}$$

Taking the natural logarithm of both sides of Equation 33 gives

$$\ell n\ j_{es} = \ell n\ j_{ep} + \frac{eV}{kT_e} \tag{34}$$

and therefore, the logarithm of the electron current to the probe in the retarding field region is a linear function of the probe voltage relative to the plasma voltage. The derivative of the logarithm of the current density at the

probe with respect to the V is

$$\frac{d\ \ell n\ j_{ep}}{dV} = \frac{e}{kT_e} \tag{35}$$

Therefore a plot on semi-log paper of the electron current as a function of the probe voltage will result in a straight line of slope e/kT_e, from which T_e may be determined. Since both electron and ion current contribute to the total probe current, the electron current is

$$I_e = I_P - I_i \tag{36}$$

The ion current is essentially constant for $V_P < V_S$ and may be extrapolated from the curve in the saturation ion current region as shown in Figure 12b, page 28.

The electron current to the probe is

$$I_e = j_{ep} A_s \exp\left(\frac{Ve}{kT_e}\right) \tag{37}$$

where A_s is the area of the sheath. If the sheath is thin compared to probe dimensions, then A_s is essentially the area of the probe. Combining Equations 32, 35 and 36 and solving for j_{ep} yields

$$j_{ep} = \frac{I_P + I_i}{A_s} \exp\left(-\frac{Ve}{kT_e}\right) = \frac{1}{4} n_{ep} e v_{ep}$$

$$= n_{ep} e \left(\frac{kT_e}{2\pi m_e}\right)^{1/2} \tag{38}$$

and from the second and fourth terms

$$n_{ep} = \frac{I_P + I_i}{eA_s}\left(\frac{2\pi m_e}{kT_e}\right)^{1/2} \exp\left(-\frac{Ve}{kT_e}\right) \tag{39}$$

All values in Equation 39 are known except the plasma electron concentration n_{ep}. To simplify, if I_P is taken as the probe current at $V_P = V_S$, then $V = V_P - V_S = 0$ and Equation 38 becomes

$$n_{ep} = \frac{I_P + I_i}{eA_s}\left(\frac{2\pi m_e}{kT_e}\right)^{1/2} \tag{40}$$

The space potential V_S is measured by locating the knee of the curve between region A and region B.

II. EXPERIMENTAL RESULTS

Static Langmuir Probe Measurements

Two essentials for obtaining accurate and repeatable Langmuir probe data are a good vacuum system and a properly constructed plasma tube. The vacuum system, shown in Figure 13, was constructed using standard high vacuum equipment. Pressures of 10^{-6} torr could be achieved by the system. A plasma tube 12 mm in diameter and approximately 60 mm long was constructed. Six tungsten probes, 5 mils in diameter and protruding approximately 2 mm into the plasma tube, were added along the tube.

Point-by-point Langmuir probe measurements were determined using the arrangement shown schematically in

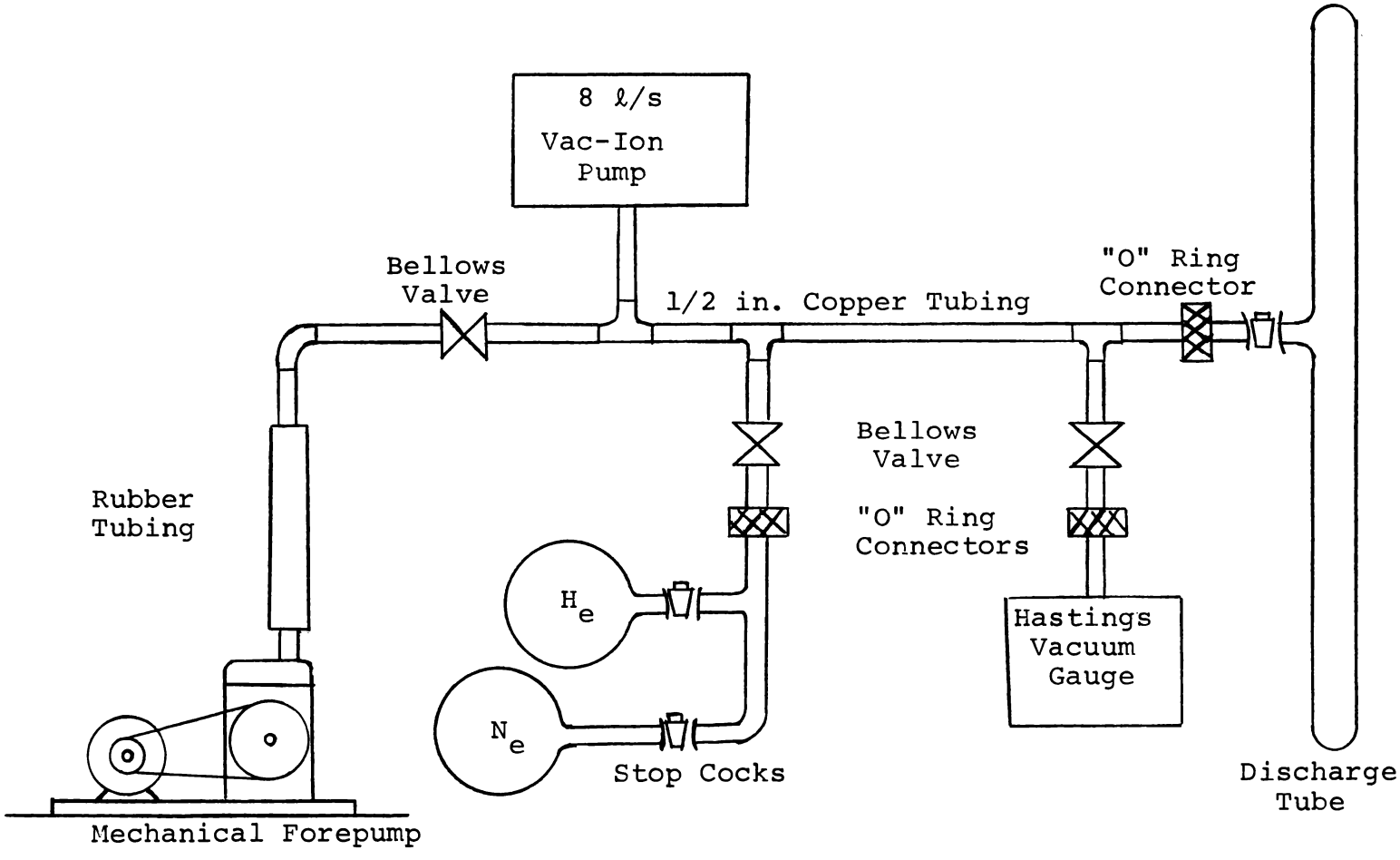

Figure 13. High vacuum system.

Figure 12a, page 28. The battery, V_B, was varied to bias the probe with respect to the plasma potential, and probe current and voltage readings were recorded. The Langmuir probe characteristic for one set of discharge parameters is shown in Figure 14. A semi-log plot of the exponential portion of the characteristic is shown in Figure 15. From the slope of this latter curve, T_e was calculated using Equation 35. Location of the knee of the curve determined the space potential V_S and, using the probe current at V_S and the probe area, electron density was calculated from Equation 40.

Swept Probe Measurements Using PCI

Intrinsic noise problems were encountered early in this investigation. It was found that this noise level varies with discharge parameters and with the gases used. Helium for example exhibited a much lower characteristic noise level than neon. A probe characteristic for neon is shown in Figure 16. Efforts were made to find pressure and discharge current combinations which would give a relatively quiet Langmuir probe characteristic. No such quiet condition was found for neon. Helium exhibited the same noisy characteristics at higher pressures, but was relatively quiet for pressures below 3 torr. The noise was found to be less than 100 kHz as reported in the literature (9). Figure 17 shows a typical probe noise spectrum for helium.

The apparatus shown schematically in Figure 18 was

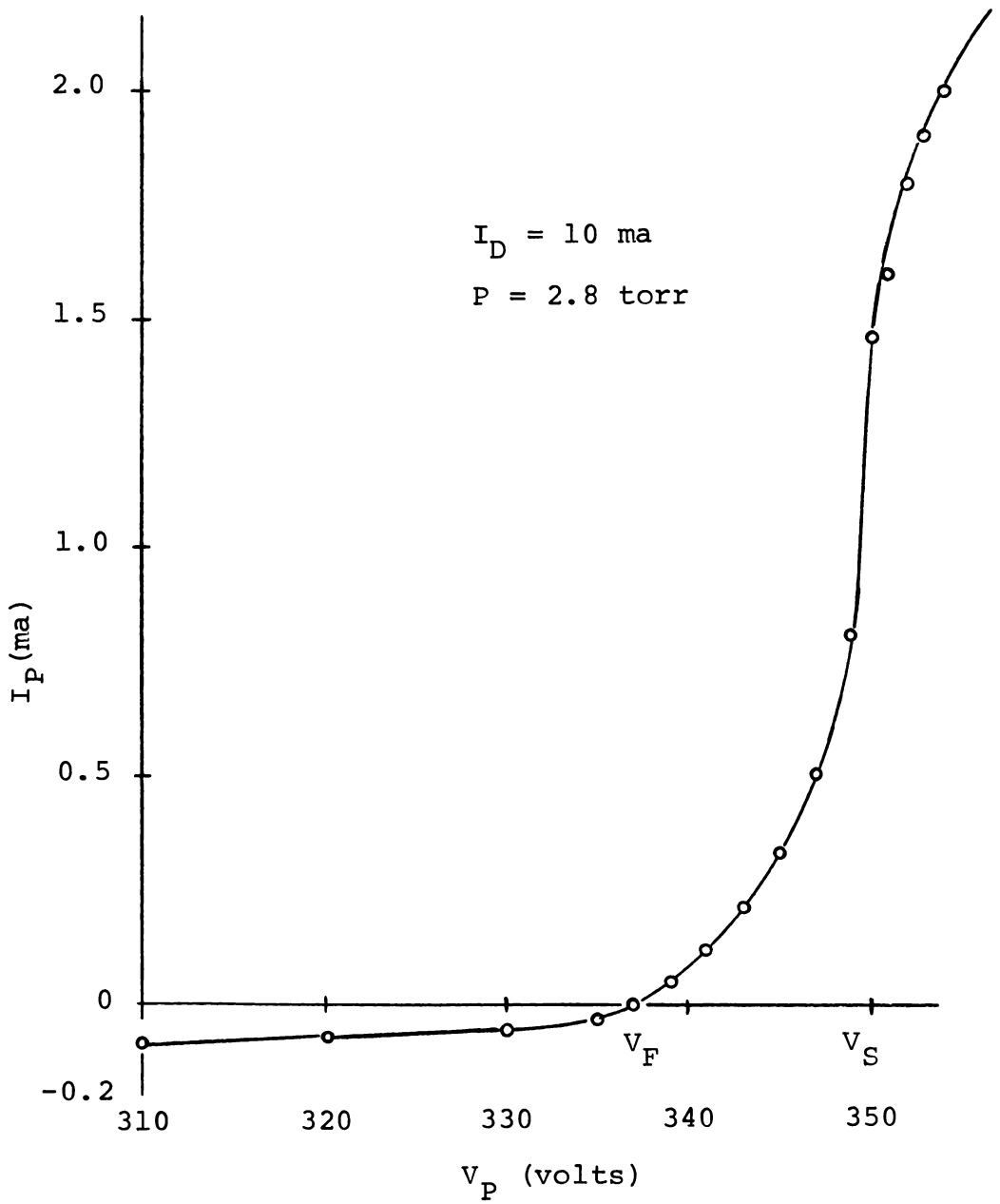

Figure 14. Static Langmuir probe characteristic for helium.

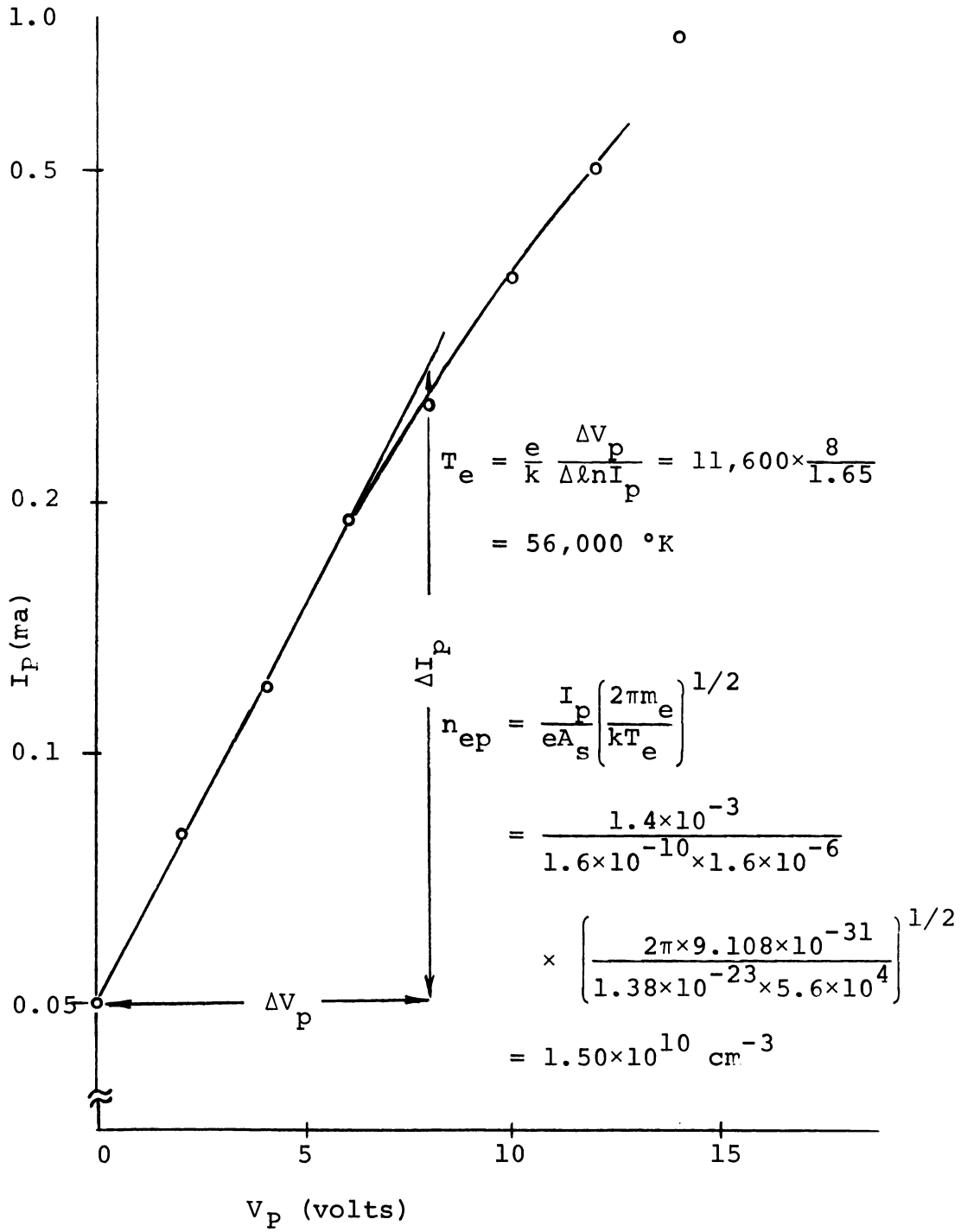

Figure 15. Semi-log plot of the exponential portion of the static Langmuir probe characteristic for helium.

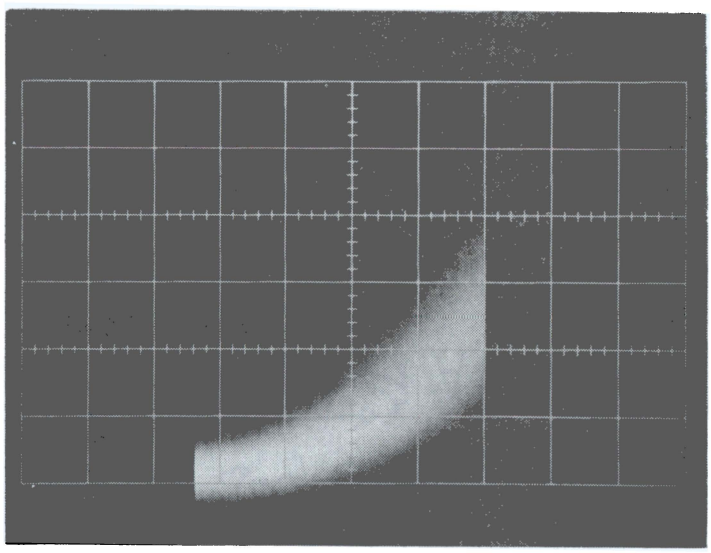

Figure 16. Typical swept probe characteristic for neon showing noise level.

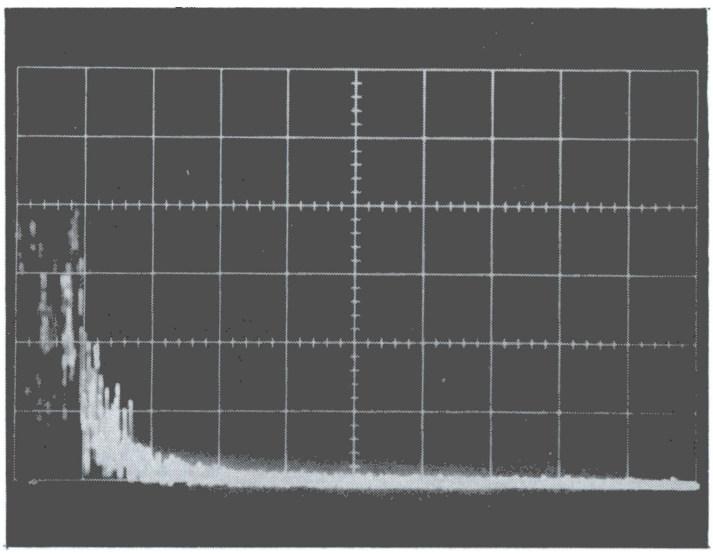

Vertical: 5 mv/cm

Horizontal: f_C = 500 kHz

f_D = 100 kHz/cm

Figure 17. Spectrum of the noise for helium.

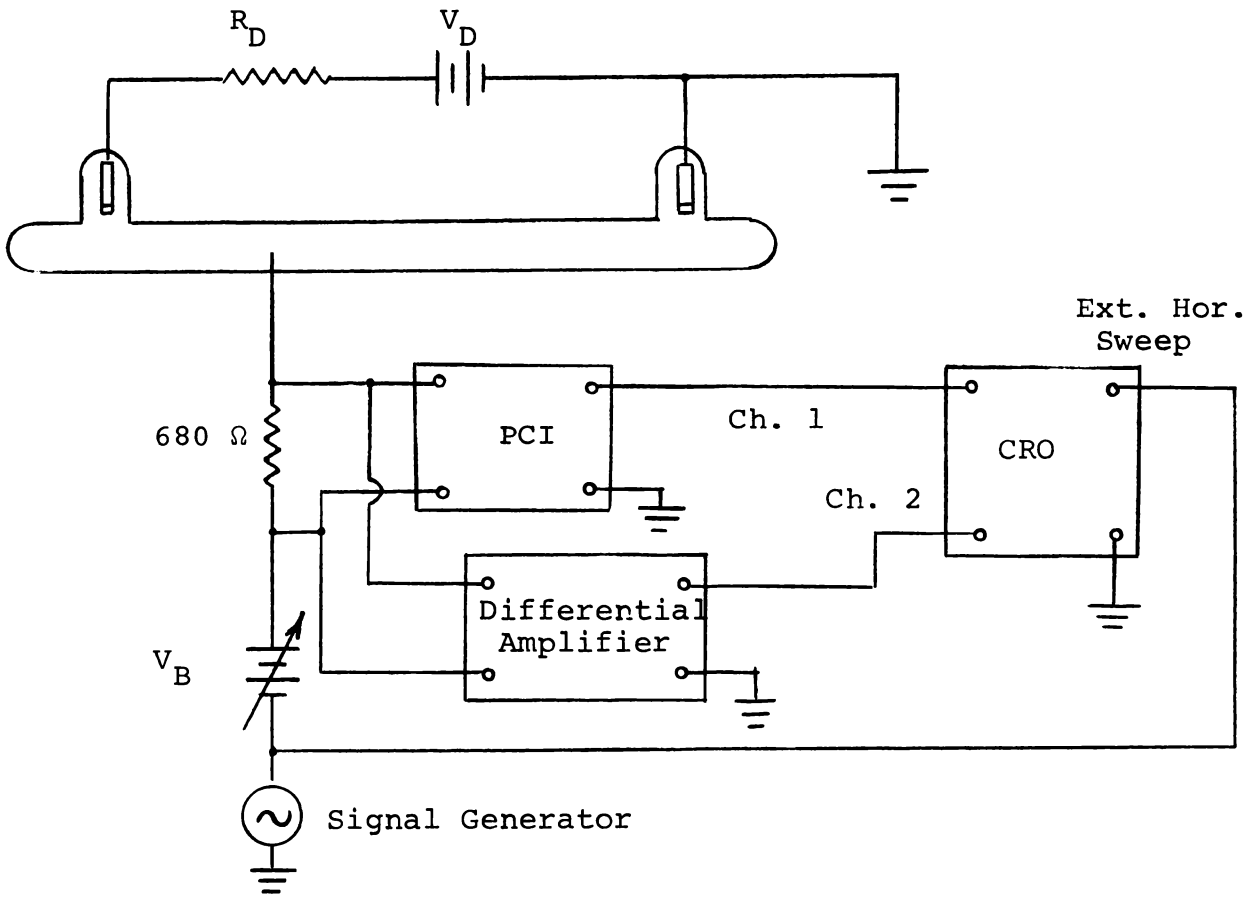

Figure 18. Schematic of the apparatus for determining the accuracy of the PCI.

used to determine the accuracy of the probe characteristic obtained with the PCI. The photograph of Figure 19 shows the differential amplifier output in the top trace and PCI output in the bottom trace. The horizontal trace was swept externally with the same 16 volt peak-to-peak sawtooth which was applied to the probe. The sweep frequency was 1 kHz. Vertical displacement for the top trace was 40 mv/cm; for the bottom, 20 mv/cm. Vertical displacement of the bottom trace is approximately 60 mv. The gain of the PCI is 0.4 and the voltage measured by the PCI is approximately 150 mv. The total vertical displacement of the top trace is approximately 145 mv and the results for the two difference methods are in good agreement. Note that the curves are at the beginning of the saturation electron region. A change of 150 mv across R_p represents a change in 0.2 ma in I_p, which is typical for this region.

Swept probe characteristics were obtained using the PCI and the oscilloscope camera. The circuit for making this measurement was the same as shown in Figure 18, but with the differential amplifier removed. Photographs of two such characteristics are shown in Figures 20 and 21. These curves are plotted on semi-log paper in Figures 22 and 23. From the exponential portion of the curve, the slope e/kT is determined and electron temperature T_e is calculated. Once T_e is known and the probe current at the space potential V_S is found from the semi-log plot, the electron density is calculated from Equation 40.

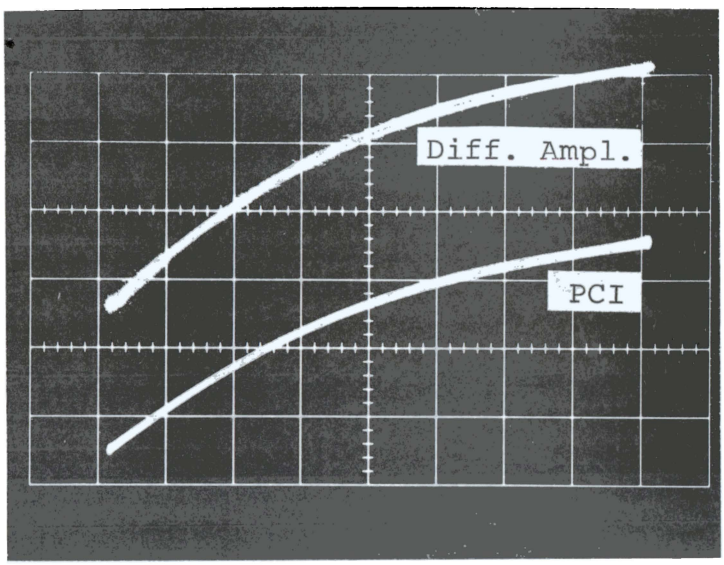

Figure 19. Dual trace showing output of the PCI and the differential amplifier.

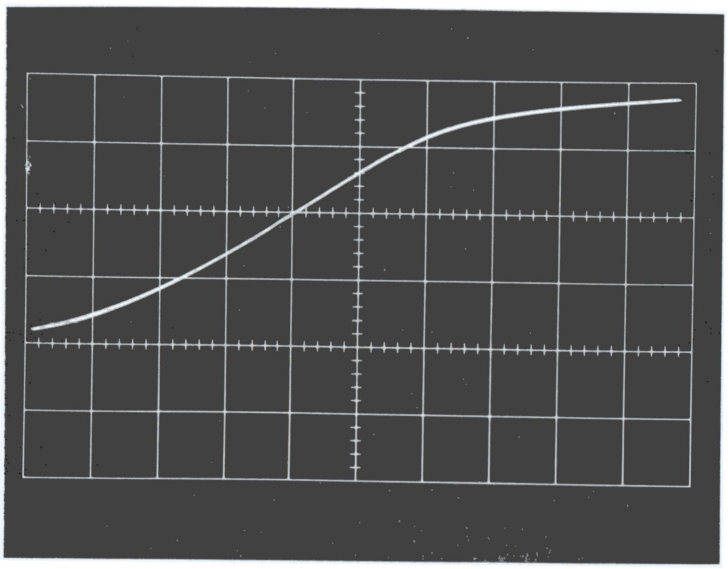

Vertical: 0.1 ma/cm

Horizontal: 2 v/cm

Figure 20. Langmuir probe characteristic for I_D = 15 ma, P = 2.45 torr.

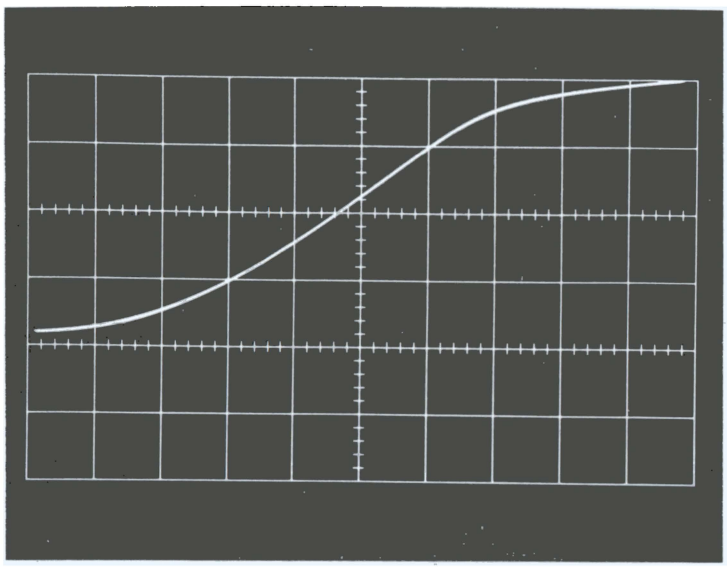

Vertical: 0.1 ma/cm

Horizontal: 2 v/cm

Figure 21. Langmuir probe characteristic for I_D = 23 ma, P = 2.45 torr.

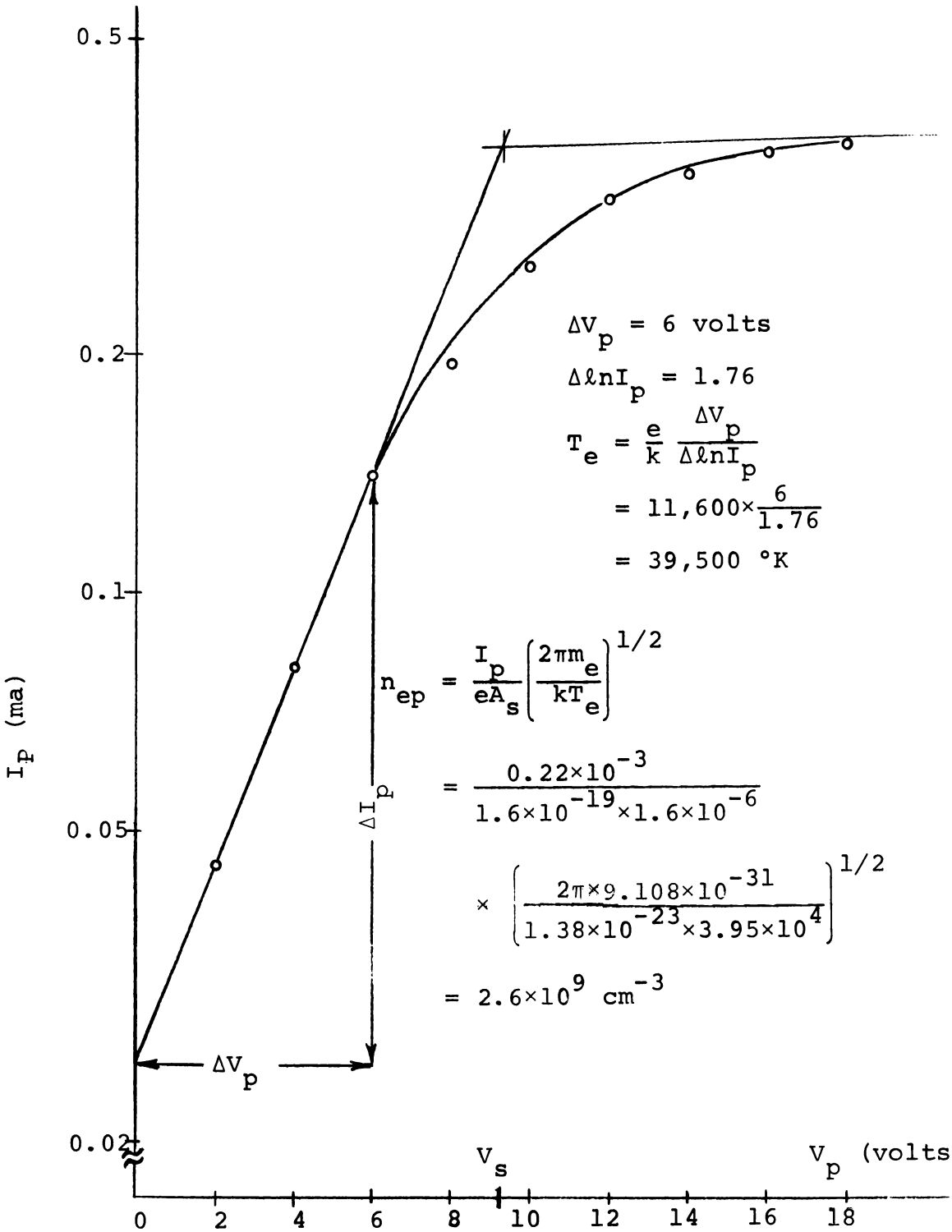

Figure 22. Semi-log plot of the exponential portion of the Langmuir probe characteristic for I_D = 15 ma.

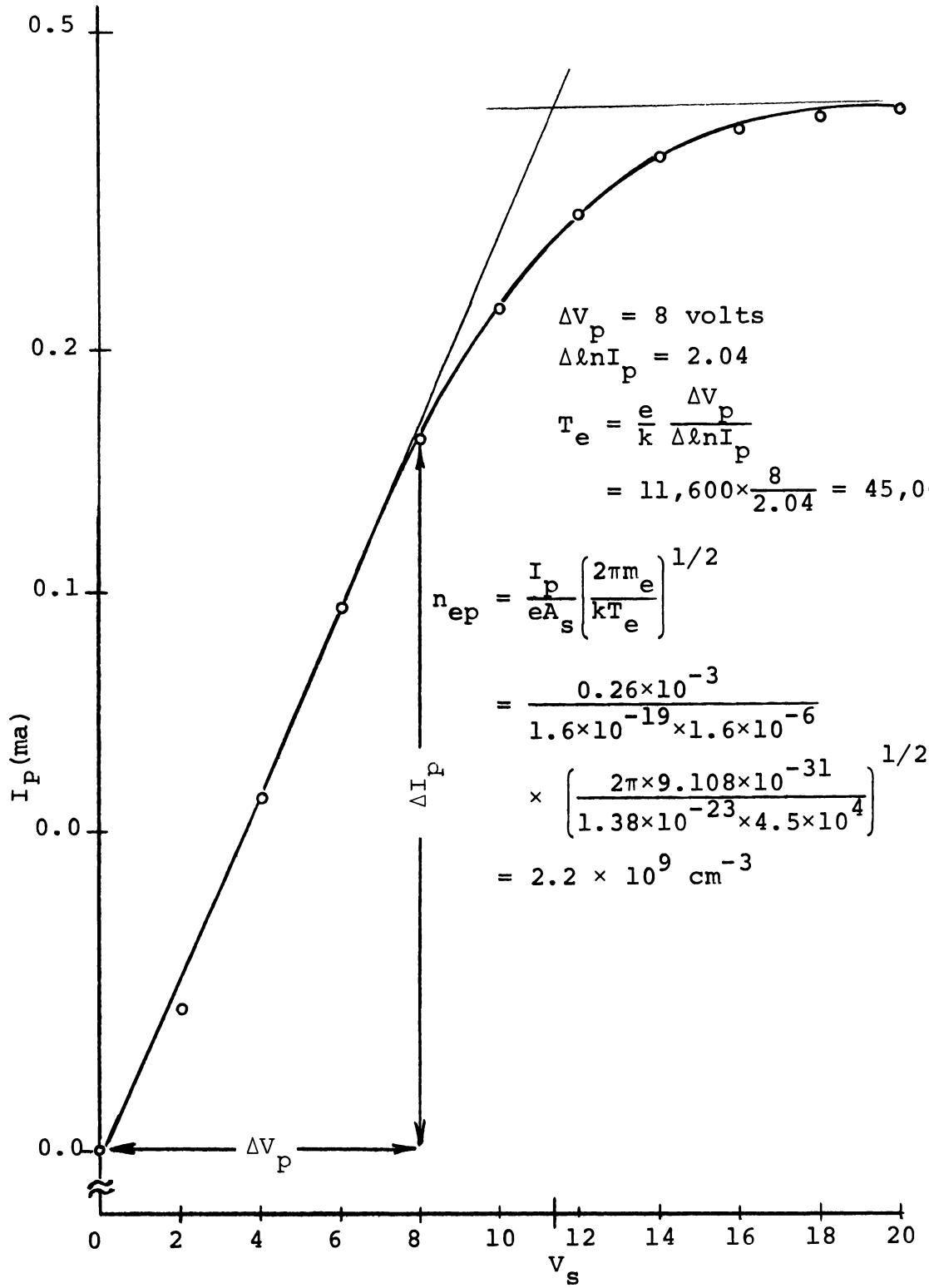

Figure 23. Semi-log plot of the exponential portion of the Langmuir probe characteristic for I_p = 23 ma.

III. DOUBLE PROBE NOISE MEASUREMENTS

The use of double probes for determining plasma parameters in the absence of a reference electrode in contact with the plasma was originally proposed by Johnson and Malter (22). The method was invented to be used in cases where the plasma potential changed with time. The two probes, biased with respect to each other, are a floating system which follows the change in plasma potential. This method used in conjunction with the photon-coupled isolator should provide both the frequency response and sensitivity to measure the inherent plasma noise.

Figure 24 shows a schematic of the apparatus used for making double probe measurements. The voltage drop across the 100 KΩ resistor represents the fluctuations in plasma potential. Figure 25 is a plot of probe noise voltage versus pressure between probes one and five for various discharge currents in helium. Figure 26 shows the probe noise versus discharge current between probes one and five as the pressure is varied. Figure 27 shows variations in noise voltage as a function of distance along the plasma tube, for neon. A constant discharge current of 10 ma was maintained for these measurements. The reference probe was probe number five, nearest the anode end of the tube. The curves show a pressure for which noise is a minimum, in this case approximately 1.75 torr. The curves also show a large rise in noise as the cathode is approached.

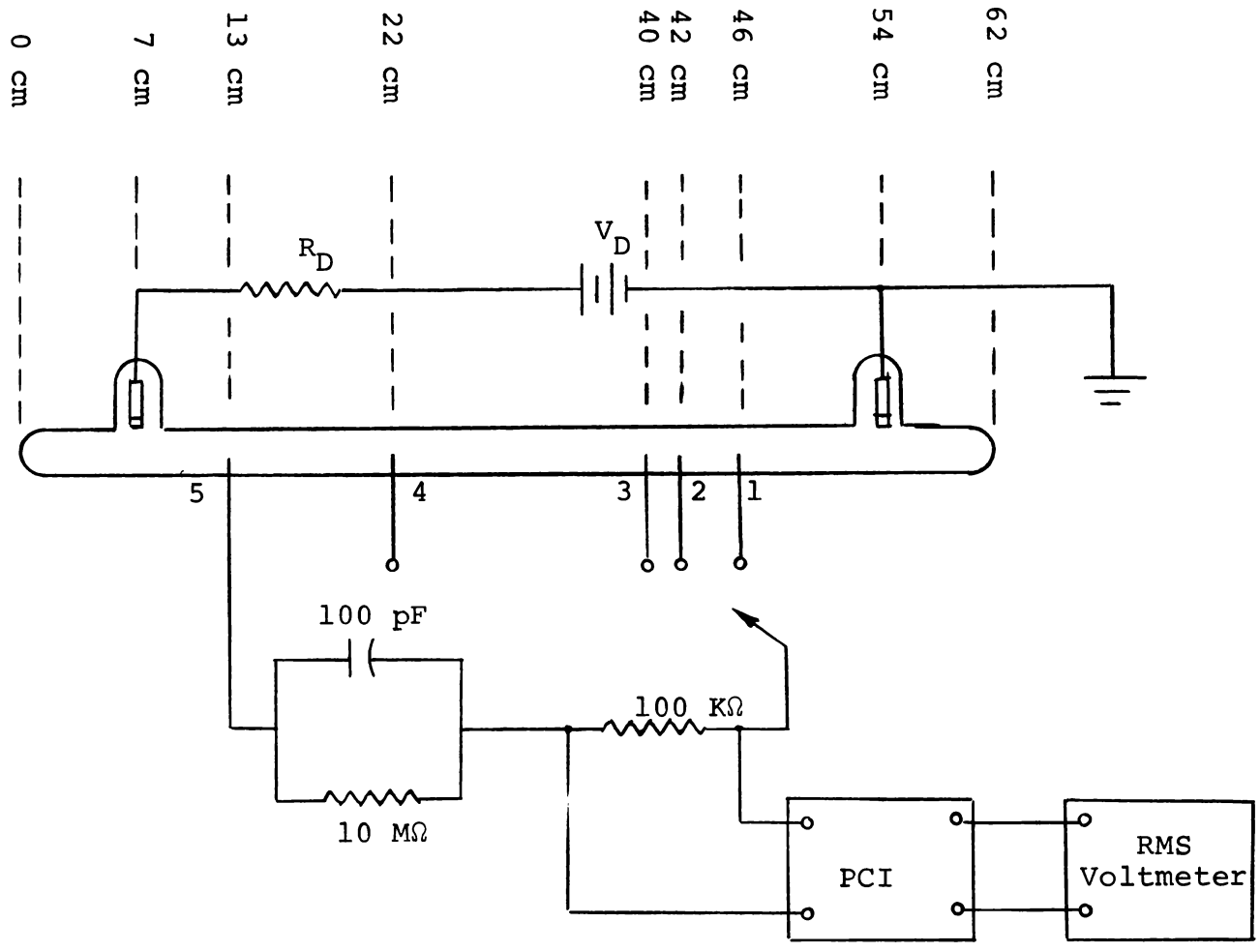

Figure 24. Circuit for measuring double probe noise characteristics.

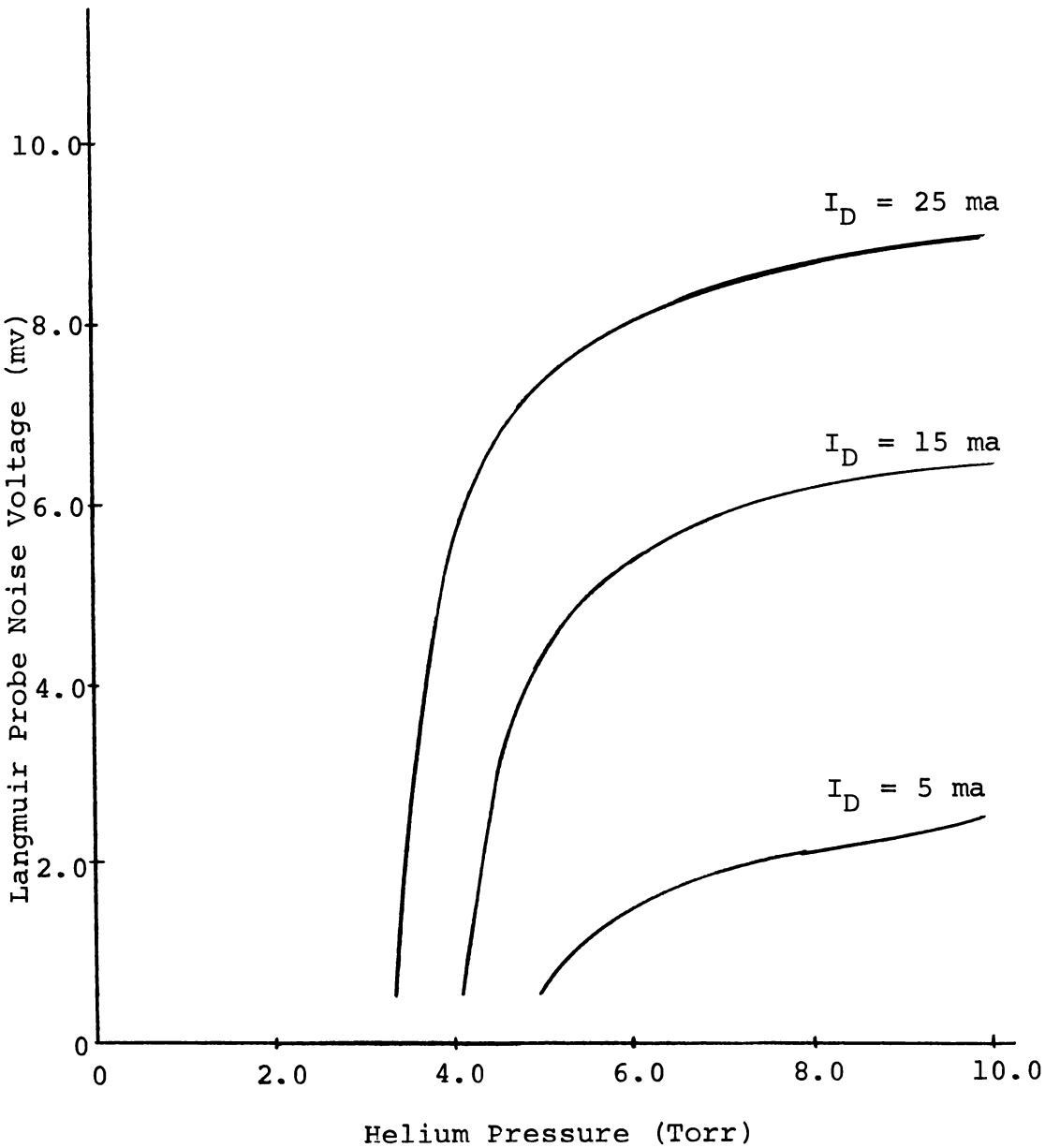

Figure 25. Langmuir probe noise voltage versus helium pressure.

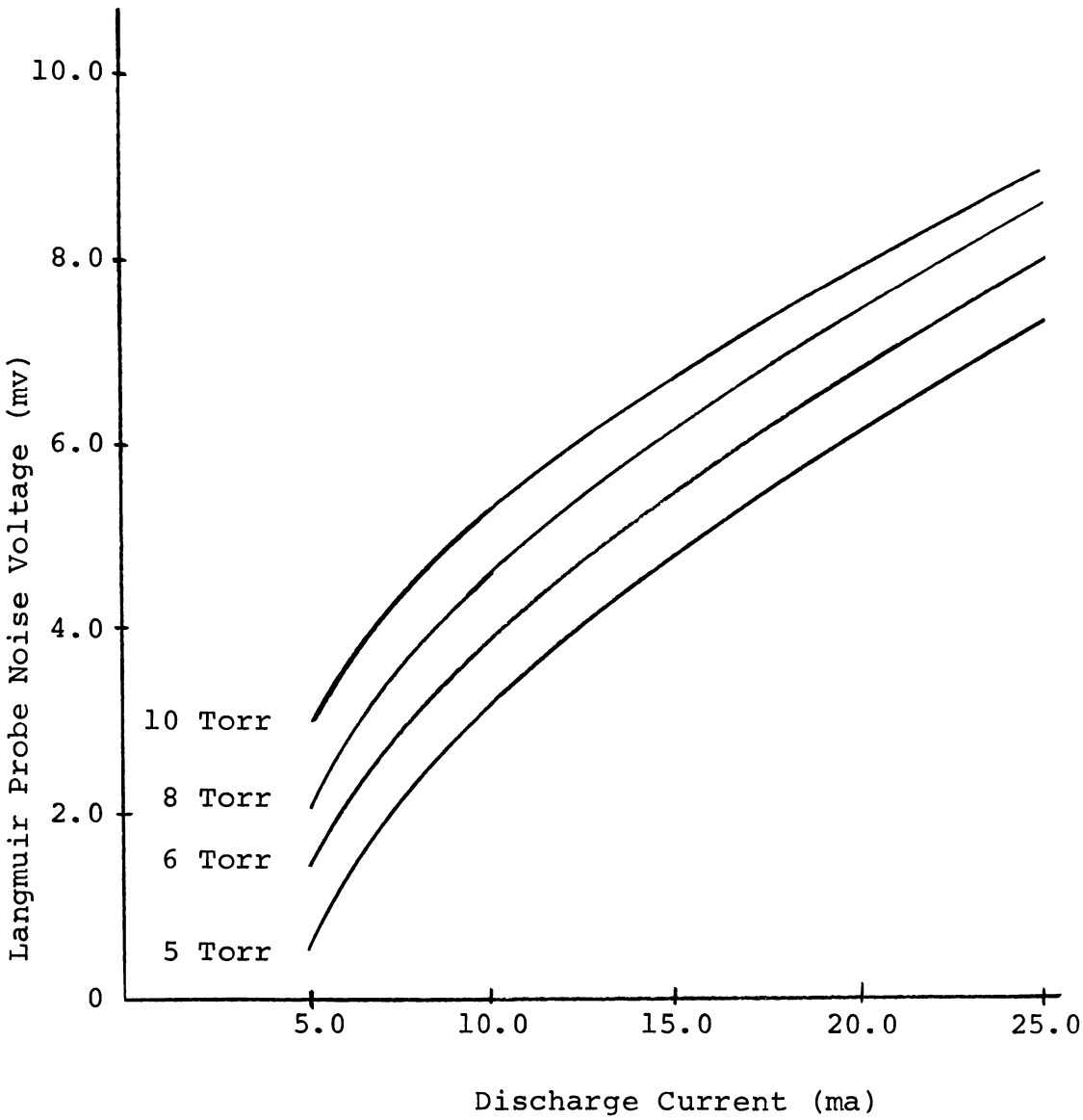

Figure 26. Langmuir probe noise voltage versus discharge current for helium.

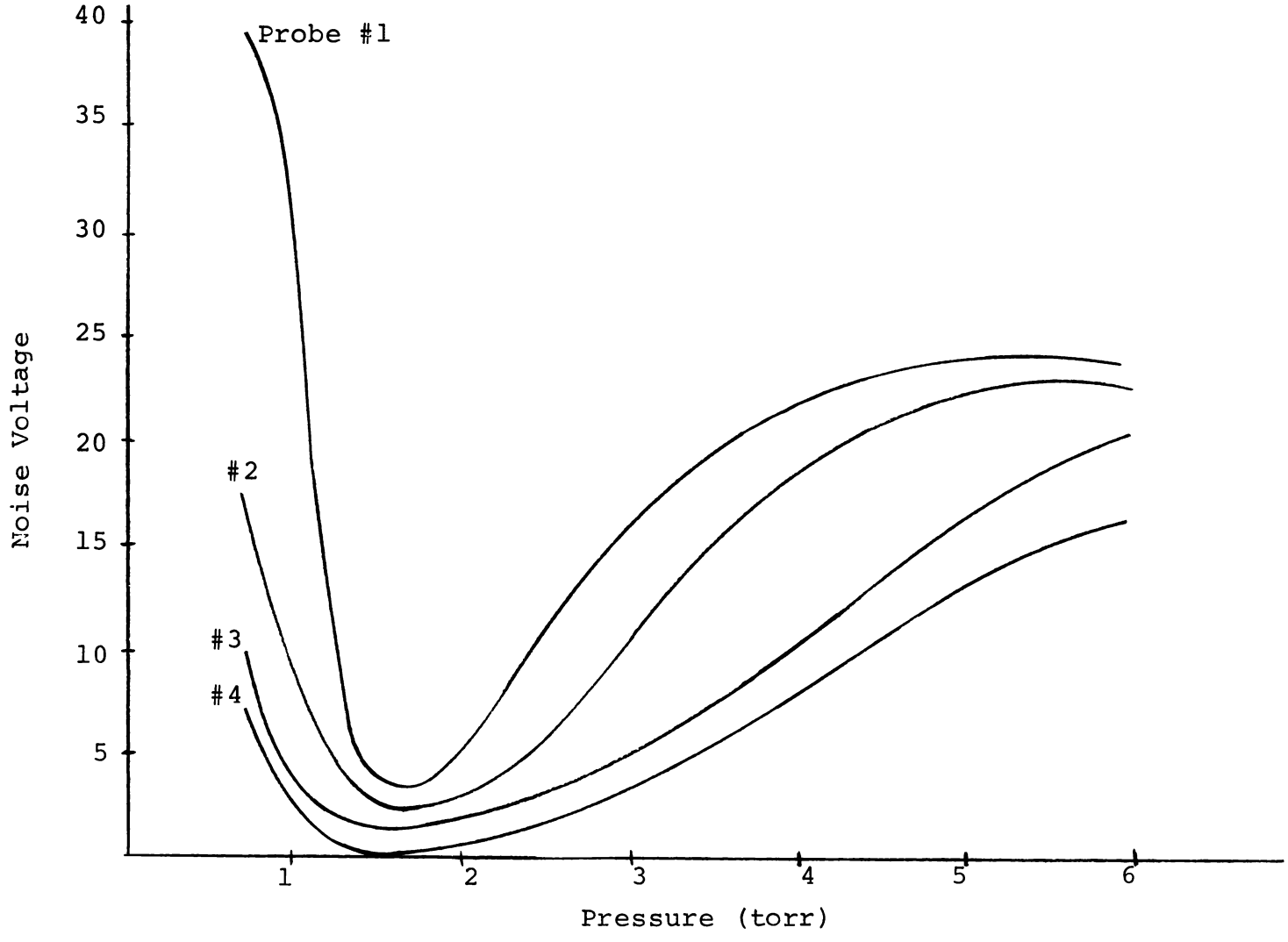

Figure 27. Langmuir probe noise voltage versus helium pressure.

CHAPTER IV

CONCLUSIONS

The photon-coupled isolator circuit combines an FET, an LED, a PIN photodiode, and a bipolar transistor in an amplifier which provides the isolation and frequency response needed for swept Langmuir probe plasma diagnostics. The performance of the circuit is indicated by the gain and frequency response curve of Figure 10, page 24. Investigation thus far indicates that the thermal instability of the photon-coupled isolator is the major limitation of the amplifier. Development of a compensation network to provide thermal stability is the subject of another investigation

In addition to the four devices used in the amplifier, this study has considered two additional devices, the Langmuir probe and the plasma tube itself, in developing instrumentation for plasma diagnostics. Swept probe characteristics can be displayed and recorded in less than one second to insure collection of data prior to probe contamination. The instrumentation exploits the good transient response of the probe in the retarding field region to provide a method of investigating fluctuations in the plasma.

Improvements to the photon-coupled isolator would include an additional stage in the preamplifier circuit to increase the gain and extend the frequency response.

BIBLIOGRAPHY

BIBLIOGRAPHY

1. Cobine, J. D. "Introduction to Volume 4," The Collected Works of Irving Langmuir, G. Suits, editor. Vol. 4. New York: The Macmillan Company, 1961. Pp. xvi-xxi.

2. Garrett, C. G. B. Gas Lasers. New York: McGraw-Hill Book Company, Inc., 1967.

3. Mather, N. W., and G. W. Sutton. Engineering Aspects of Magnetohydrodynamics. New York: Gordon and Breach Science Publishers, 1964.

4. Cobine, J. D. Gaseous Conductors. New York: Dover Publications, Inc., 1958.

5. Huddlestone, R. H., and S. L. Leonard. Plasma Diagnostic Techniques. New York: Academic Press, Inc., 1965.

6. Wehner, G., and G. Medicus. "Reliability of Probe Measurements in Hot Cathode Gas Diodes," Journal of Applied Physics, 23:1035-1046, September, 1952.

7. Bunning, W. D., Jr., and W. J. Heikkila. "Observations on the Effect of Surface Conditions on Langmuir Probes," Journal of Applied Physics, 41:2263-2264, April, 1970.

8. Bills, D. G., R. B. Holt, and B. T. McClure. "Pulsed Probe Measurements," Journal of Applied Physics, 33:29-33, January, 1962.

9. Shofner, F. M., C. W. Bray, and T. B. Carlson. "Investigation of Noise Characteristics and Amplitude Stabilization of Plasma Lasers." Report prepared under NASA Contract No. NGL-43-001-056 by The University of Tennessee Space Institute, Tullahoma, Tennessee, August, 1970.

10. Shofner, F. M. "A Circuit for the Convenient and Rapid Oscillographic Display of Langmuir Probe Data." Unpublished Master's thesis, The University of Tennessee, Knoxville, 1964.

11. Welch, J. L. "An Investigation of a Temperature-Stabilized, Photon-Coupled, Isolator-Preamplifier Circuit." Unpublished Master's thesis, The University of Tennessee, Knoxville, 1968.

12. Photon Coupled Isolators HP 5081-4300 Series. Palo Alto, California: Hewlett Packard Associates, 1968.

13. Preferred Semiconductors and Components from Texas Instruments. Dallas, Texas: Texas Instruments, Inc., 1969.

14. Sevin, L. J. Field-Effect Transistors. New York: McGraw-Hill Book Company, Inc., 1965.

15. Todd, C. E. Junction Field-Effect Transistors. New York: John Wiley and Sons, Inc., 1968.

16. Angelo, E. J. Electronics: BJTs, FETs, and Microcircuits. New York: McGraw-Hill Book Company, Inc., 1969.

17. Electrical Isolation Using the HPA 4310. Palo Alto, California: Hewlett Packard Associates, 1967.

18. Pierce, J. F. Transistor Circuit Theory and Design. Columbus, Ohio: Charles E. Merrill Books, Inc., 1963.

19. Langmuir, I., and H. Mott-Smith. "Studies of Electric Discharges in Gases at Low Pressures," The Collected Works of Irving Langmuir, G. Suits, editor. Vol. 4. New York: The Macmillan Company, 1961. Pp. 23-98.

20. Langmuir, I., and H. Mott-Smith. "The Theory of Collectors in Gaseous Discharges," The Collected Works of Irving Langmuir, G. Suits, editor. Vol. 4. New York: The Macmillan Company, 1961. Pp. 99-132.

21. Tonks, L., and I. Langmuir. "A General Theory of the Plasma of an Arc," The Collected Works of Irving Langmuir, G. Suits, editor. Vol. 4. New York: The Macmillan Company, 1961. Pp. 176-224.

22. Johnson, E. O., and L. Malter. "A Floating Double Probe Method for Measurements in Gas Discharges," Physical Review, 80:58, October, 1950.

VITA

Roy L. Heifner, Jr. was born in Oxford, Alabama, on February 18, 1938. He graduated from Oxford High School in 1956. He received a Bachelor of Electrical Engineering degree from Auburn University in 1962.

He received a commission through the Army Reserve Officers Training Corps program at Auburn and served two years with the Army. From 1965 to 1969 he was employed by The Boeing Company in Huntsville, Alabama, as a Design Engineer with the Saturn V Project.

In the fall of 1968, he was selected by Boeing as a candidate for a Research Fellowship at The University of Tennessee Space Institute and in January, 1969, accepted a position as Research Fellow with the Institute. He received the Master of Science degree in Electrical Engineering in 1971.

He is married to the former Patricia Ann Reaves of Oxford, Alabama. They have a ten year old daughter, Lisa Ann.